RSC Advances

PAPER

View Article Online
View Journal | View Issue

Check for updates

Cite this: *RSC Adv.*, 2024, **14**, 20809

Optimization of silver nanoparticles synthesis *via* Plackett–Burman experimental design: *in vitro* assessment of their efficacy against oxidative stress-induced disorders†

Madiha Muhammad Fazil,[b] Anum Gul *[a] and Huma Jawed[b]

Nanoparticles possess remarkable biological activities owing to their small size and large surface-to-volume ratio. Given the increasing adoption of environmentally sustainable practices in silver nanoparticle (AgNP) fabrication, this study presents a simple lab-scale green synthesis of AgNPs using banana peels. Large amounts of banana peels are disposed off in Pakistan every day. As the fruit is available throughout the year and contains many active components with potent biological activities, we aimed to synthesize silver nanoparticles using its peel, through an energy-efficient and inexpensive route. The synthesis was optimized according to the Plackett–Burman design (PDB) of experiments, which helped identify significant factors and saved time and resources. For characterization, UV-Vis spectroscopy and SEM-EDX analysis were performed, revealing spherical particles in the 45–65 nm size range. To investigate functional groups, FT-IR analysis was performed, revealing the presence of N–C=O amide I bonds of proteins, C–H bonds of tannins and C–O bonds involved in the capping and stabilization of nanoparticles. The free radical scavenging property of banana peel-mediated silver nanoparticles (BP-AgNPs) was studied against 2,2-diphenyl-1-picrylhydrazyl (DPPH), and the antioxidant potential was found to be 79% at 500 μg mL^{-1} concentration. The efficacy of BP-AgNPs with respect to certain biological activities were studied through anti-inflammatory assays, which demonstrated better results compared to a standard drug, and an anti-glycation assay, wherein only 4% of AGEs were formed, demonstrating 96% of AGE inhibition *in vitro*. The findings not only demonstrated the effectiveness of the PBD approach but also highlighted the potent property of BP-AgNPs against disorders associated with oxidative stress.

Received 14th April 2024
Accepted 19th June 2024

DOI: 10.1039/d4ra02774d

rsc.li/rsc-advances

Open Access Article. Published on 01 jul 2024. Downloaded on 22.4.2026. 20.32.45.
This article is licensed under a Creative Commons Attribution-NonCommercial 3.0 Unported Licence.

1 Introduction

Nanotechnology has been profoundly used in practically all domains of science, and nanomaterials have been used in numerous ways owing to their distinctive properties. The high surface-to-volume ratio is the chief reason for their efficacy because particles experience major changes in their physical, chemical and biological properties at the nanoscale.[1] Nanoparticles can be synthesized using metal precursors of nearly all metals; the well-known metals include gold, silver, iron, copper, lead, zinc, cobalt, aluminum, cadmium and selenium, but silver nanoparticles are of more interest considering their unique electrical, optical and magnetic properties.[2] Nanoparticles are being successfully utilized in novel applications in the field of molecular imaging, targeted drug delivery, coatings, cancer therapy, catalysis, cosmetics[3] nanomedicine,[4] wastewater remediation, disinfecting agents,[5] agriculture for nano-formulated pesticides and nanosensors for disease identification.[6]

The emerging area of modern nanotechnology called nanobiotechnology involves the fabrication of nanoparticles using naturally occurring substances from plants, algae, fungi and bacteria.[2] This green synthesis is a viable substitute for traditional reduction techniques that call for natural compounds with dual behavior as capping and reducing agents. Physical synthesis requires high energy consumption, high cost, low yield and uneven distribution, whereas chemical methods utilize expensive and hazardous chemicals.[3,7] In contrast, the utilization of biological systems offers several advantages, including the availability of an extensive and inexpensive choice of biological assets, shorter production time and ease of fast solubility of nanoparticles in water.[1,8]

The inclusion of plants in the formation of silver nanoparticles has gained interest due to its quick, non-pathological,

[a]*Dow College of Biotechnology, Dow University of Health Sciences, Karachi, Pakistan. E-mail: anum.gul@duhs.edu.pk; gul_anum@yahoo.com*

[b]*Department of Biosciences, Mohammad Ali Jinnah University, Karachi, Pakistan*

† Electronic supplementary information (ESI) available. See DOI: https://doi.org/10.1039/d4ra02774d

© 2024 The Author(s). Published by the Royal Society of Chemistry

Open Access Article. Published on 01 jul 2024. Downloaded on 22.4.2026. 20.32.45.
This article is licensed under a Creative Commons Attribution-NonCommercial 3.0 Unported Licence.

one-step method for biosynthetic processes and budget-friendly protocol. The combination of biomolecules found in plant extracts, including phytochemicals, polysaccharides, proteins, and enzymes, contributes to the reduction and stabilization of nanoparticles. These compounds, while chemically complex, also offer various medicinal benefits.[9] Notably, fruit peels are reported to have three times the amount of polyphenolic chemicals as fruit flesh.[10] Peels are typically discarded as waste by the fruit processing industry yet contain a wealth of bioactive compounds, including phenols, tannins, flavonoids, carotenoids, steroids, vitamins and essential oils, all of which have significant health benefits.[11] The presence of such valuable biomolecules in fruit peels makes them a perfect candidate for use in the development of a variety of highly structured hierarchical nanostructures of diverse sizes and forms. One of the most popular fruits with a lot of nutrients is banana and its peels instinctively have an abundance of polymers.[10,12]

The optimization of nanoparticles is carried out manually applying various conditions one at a time in most studies, which is time-consuming. However, the Plackett–Burman Design-Design of Experiments (PBD-DoE) could accomplish this task more effectively and quickly. DoE is a widely recognized and effective statistical tool to optimize the processes and bring improvement in scientific domains.[13] Plackett Burman Design (PBD) is a type of fractional factorial design that operates under the idea that interactions can be fully disregarded and the main effects can be calculated using minimal experiments. It is a very effective screening design that can optimize all the influencing factors together to get over the challenges of a single-factor optimization approach. It offers a quick way to select the critical variables from a vast pool of variables, saving time with less process variability and reduces overall expenses.[14]

Nanomedicines have the potential to address a number of medical complications; they have demonstrated an improved ability to bind with biomolecules and reduce oxidative stress and inflammation in tissues.[15] Glycation, inflammation, and reactive oxygen species (ROS) are interrelated processes that have a significant impact on a number of physiological and pathological states. Highly reactive chemical species known as reactive oxygen species (ROS) are the by-products that naturally occur as the result of cellular metabolism. Excessive ROS generation or inadequate antioxidant defense mechanisms might result in oxidative stress. Inflammation is also known to arise as a result of oxidative stress, activating a number of inflammatory pathways and promoting the pro-inflammatory cytokines, adhesion molecules and chemokines production.[16] Reactive oxygen species can also accelerate the glycation process by oxidizing carbohydrates, increasing the irreversible production of advanced glycated end products (AGE). Increased glycation and AGEs buildup contributes to the structural and functional degradation of biomolecules and plays a significant role in the pathophysiology of diabetes, aging process and different cancers.[17] Therefore, the present study aims to screen phytochemicals in banana peels extract, synthesize silver nanoparticles through PBD optimization and assess their capability against oxidative stress-related complications.

2 Methodology

2.1 Reagents

Disodium hydrogen phosphate, sodium dihydrogen phosphate, $FeCl_3 \cdot 6H_2O$, DPPH, fructose, iodine, nitric acid, H_2SO_4, and HCl were sourced from Sigma-Aldrich. L-ascorbic acid, isopropyl alcohol, and $AgNO_3$ were obtained from Daejung. NaCl was purchased from Riedel-de-Haën. Sodium azide was purchased from VWR Chemicals and BSA from BDH Laboratory. All the chemicals used in this study were of analytical grade, ensuring high purity and quality for precise and reliable experimental results.

2.2 Banana peels extract preparation

For the extract preparation, banana peels were obtained and cleaned well to get rid of any dust particles. Then the peels were dried in a hot-air oven at 70 °C, crushed into a fine powder using a grinder and stored in an airtight container. 2.5 g of the crushed powder was added to 50 mL of Milli-Q water and boiled for 10 min. After heating, the solution was sieved and centrifuged for 20 min at 5000 rpm to obtain the clear peel extract. The aqueous extract was stored at 4 °C till further use.

2.3 Qualitative phytochemical screening

Various tests were conducted to detect specific compounds in banana peels extract. Alkaloids were detected by adding a few drops of iodine to 3 mL of the banana peels extract; the solution was boiled and observed for a blue color formation.[18] The xanthoproteic test was employed for proteins and amino acids, which involved mixing concentrated nitric acid with the plant extract. Nitric acid reacts to introduce nitro groups into the aromatic rings of proteins, thus changing the solution color.[19] Tannins and phenols were screened by adding 1 mL of the extract with a few drops of 2% $FeCl_3$ as phenols and tannins reduce it to form colored complexes.[19] Flavonoids in banana peels were assessed by adding a few drops of concentrated H_2SO_4 in 1 mL of the extract, changing the color to yellow or orange color.[20] For tannins detection, 1 mL of the extract was mixed with 1 mL of distilled water, and a few drops of 10% $FeCl_3$ were added to check for precipitation.[21] Phlobatannins were detected by boiling 2 mL of the aqueous extract with the same amount of 1% HCl to observe a color change and precipitation.[2,21] Quinones were tested by dissolving 10 mg of banana peel powder in isopropyl alcohol and adding a drop of concentrated H_2SO_4 to note a red color change.[22] Salkowski test for phytosterols involved combining 5 mL of aqueous extract with 2 mL of concentrated H_2SO_4 and 2 mL of chloroform to observe the presence with a pink ring or red color in the lower chloroform layer.[18] Saponins were screened by boiling 1 mL of the fruit peel extract with 10 mL of Milli Q water for 15 minutes and shaking upon cooling. To reduce surface tension saponins make foam after vigorous shaking, marking their presence.[2] Finally, Benedict's test confirmed the presence of carbohydrates (reducing sugars) by mixing the aqueous plant extract with 0.5 mL of Benedict's reagent and boiling for 2 minutes as they reduce copper ions to form a colored solution.[20]

© 2024 The Author(s). Published by the Royal Society of Chemistry

Open Access Article. Published on 01 jul 2024. Downloaded on 22.4.2026. 20.32.45.
This article is licensed under a Creative Commons Attribution-NonCommercial 3.0 Unported Licence.

Table 1 Parameters with low and high levels

Parameters	Low (−1)	High (+1)	Centre (0)
$AgNO_3$ concentration	1 mM	5 mM	3 mM
Incubation temperature	25 °C	50 °C	37.5 °C
Incubation time	0.5 hours	2 hours	1.25 hours
Plant-to-$AgNO_3$ ratio	1 : 1	1 : 10	1 : 5.5

2.4 Optimization of AgNPs synthesis using Plackett–Burman Design

The synthesis of AgNPs was optimized using Plackett–Burman Design on Minitab 17 software. Four parameters were selected with 2 levels and 1 center point (Table 1) for the generation of the optimization reactions by the software. The levels denote the low and high value of each parameter used in the optimization. The PBD generated 39 runs for the optimization where 3 replicates of each reaction were given a random run in order to avoid bias. The reactions were carried out according to the DOE design, and the spectra were taken from 300 nm to 800 nm. ANOVA and regression analysis were applied for the selection of the reaction.

2.5 Biosynthesis of banana peels AgNPs (BP-AgNPs)

The banana peels extract-mediated AgNPs were synthesized according to the reaction parameters of the Plackett Burman design mentioned in Table 1. The extract was combined in different ratios with aqueous $AgNO_3$ solution in the final concentration as per the run in the PBD design (Table 2). The reaction vial was incubated at different temperatures and times according to the PBD design for the observation of color change.

2.6 Characterization of banana peels AgNPs (BP-AgNPs)

2.6.1 Spectroscopy. The bio-reduction of silver ions by banana peels extract was analyzed by the plasmon resonance

Table 2 Response for the Plackett Burman design

Run order	Incubation time (hours)	Incubation temperature (°C)	$AgNO_3$ concentration (mM)	Plant extract : $AgNO_3$
1	0.5	25	1	10
2	2	25	1	1
3	0.5	25	1	1
4	0.5	25	1	10
5	2	25	1	1
6	2	25	5	10
9	2	25	5	1
13	2	25	5	1
14	0.5	25	1	1
17	0.5	25	5	10
22	0.5	25	5	10
27	0.5	25	1	10
28	0.5	25	1	1
31	0.5	25	5	10
33	2	25	5	1
34	2	25	1	1
38	2	25	5	10
39	2	25	5	10
7	1.25	37.5	3	5.5
8	1.25	37.5	3	5.5
11	1.25	37.5	3	5.5
10	0.5	50	5	1
12	2	50	1	10
15	0.5	50	1	1
16	2	50	1	10
18	0.5	50	5	1
19	2	50	1	10
20	2	50	1	10
21	2	50	5	1
23	0.5	50	5	10
24	0.5	50	5	10
25	0.5	50	1	1
26	2	50	1	10
29	0.5	50	1	1
30	0.5	50	5	1
32	2	50	5	1
35	2	50	5	1
36	0.5	50	5	10
37	2	50	1	10

Open Access Article. Published on 01 jul 2024. Downloaded on 22.4.2026. 20.32.45.
This article is licensed under a Creative Commons Attribution-NonCommercial 3.0 Unported Licence.

property of BP-AgNPs. The UV-Vis spectrum of AgNPs solution was taken in the range from 300 nm to 800 nm on an Epoch microplate reader.

2.6.2 Scanning electron microscopy and EDX. Scanning electron microscopy imaging technique provides high-resolution images that allow for the detailed examination of the morphology and structure of BP-AgNPs. Energy dispersive X-ray spectroscopy (EDX) was conducted for the identification and quantification of the elements present in the sample. SEM-EDX provides valuable insights into the physical characteristics and composition of BP-AgNPs, which was conducted at Dow Dental College, Dow University of Health Sciences, Karachi, Pakistan using SEM JSM IT100. For the analysis, the sample was prepared by washing the nanoparticles pellet, completely drying it and then crushing it into a fine powder.

2.6.3 Fourier transform infrared spectroscopy. The functional groups on the surface of nanoparticles were identified using a Cary 630 FTIR spectrometer. AgNPs solution was centrifuged at 10 000 RPM for 20 minutes to prepare the sample, which was subsequently washed twice with Milli-Q water. Absolute ethanol was used for a final rinse to clean the remaining impurities. The pellet was air-dried and FT-IR assessment was conducted in the range of 3500–600 cm^{-1}.

2.7 Stability analysis

The stability analysis of the BP-AgNPs was performed through UV-Vis spectra at room temperature and at 4 °C. The BP-AgNPs solution was centrifuged at 10 000 rpm for 20 min and washed twice with Milli-Q water to remove the banana peels extract to stop the reduction reaction. After that, the solution was re-suspended in the same volume of Milli-Q water as the initial; half of the sample was kept at room temperature and half at 4 °C. The spectrum was taken every third day for 60 days to check the stability at different temperatures over time.

2.8 Antioxidant activity against DPPH

For the biological activities, banana peels-assisted silver nanoparticles (BP-AgNPs) were tested in the range of concentration from 500 μg mL^{-1} to 100 μg mL^{-1} made from the stock solution. The 2,2-diphenyl-1-picrylhydrazyl (DPPH) test was employed to assess the free radical scavenging property of BP-AgNPs in accordance with Alsahli *et al.*, 2021,[23] with minor modification. This test involves the measurement of the ability of BP-AgNPs to neutralize the DPPH radical, which is a stable free radical. In a 96-well plate, 100 μL of 0.2 mM DPPH solution (prepared in 95% ethanol) was combined with 100 μL of BP-AgNP (500–100 μg mL^{-1}). The mixture was then left at room temperature for 30 minutes in the dark. Through the changes in absorbance or colorimetric shifts measured at 517 nm with the spectrophotometer, the efficacy of BP-AgNPs in scavenging free radicals was determined. The control was made with DPPH and water in place of AgNPs and ascorbic acid (500 μg mL^{-1}) was used as the standard.

The percentage of free radical scavenging activity was determined using the following formula:

$$\text{Radical scavenging percentage} = \left(\frac{\text{Absorbance of the control} - \text{Absorbance of the test}}{\text{Absorbance of the control}}\right) \times 100$$

2.9 *In vitro* anti-inflammatory activity

2.9.1 Protein denaturation inhibition. Non-steroidal anti-inflammatory medications, such as ibuprofen and aspirin, are said to be able to inhibit the heat-induced denaturation of proteins at a pathological pH of 6.2–6.6. The commonly used model protein for such evaluations in research is Bovine Serum Albumin (BSA). Therefore, using the Rahmani *et al.*, 2022 method, the anti-inflammatory activity of BP-AgNPs along with aspirin (500 μg mL^{-1}) as a reference drug was investigated.[24] Briefly, 500 μL of varying concentrations (500–100 μg mL^{-1}) of BP-AgNPs were added to 500 μL of 1% aqueous BSA in sodium phosphate buffer pH 6.6. After incubation at 37 °C for 20 minutes, the mixtures were subjected to an additional heating at 72 °C for 20 minutes. Subsequently, when the tubes cooled down, the turbidity of the samples was measured using a spectrophotometer at a wavelength of 660 nm with a buffer blank. BSA alone in buffer was used as a control, and the following formula was applied to calculate the percentage of BSA denaturation inhibition.

$$\%\text{Inhibition} = \left(\frac{\text{Absorbance of the control} - \text{Absorbance of the sample}}{\text{Absorbance of the control}}\right) \times 100$$

2.9.2 Membrane stabilization test. BP-AgNPs were tested with hypo-salinity and heat stress against the erythrocytes to validate their anti-inflammatory potential.

2.9.2.1 Preparation of erythrocyte suspension. Blood was drawn from a healthy volunteer with their consent and placed in a vacutainer that contained heparin. The blood subsequently underwent 10 min of centrifugation at 3000 rpm to separate the plasma. The erythrocyte sediment was washed thrice with normal saline after the plasma was discarded. Human red blood cell (HRBC) suspension was made by reconstituting the blood with normal saline.

2.9.2.2 Inhibition of heat-induced hemolysis. 10% Human Red Blood Cells (HRBC) solution in normal saline was prepared for this assay. The test solution was prepared by adding 500 μL of 10% HRBC suspension and 500 μL of BP-AgNPs (500–100 μg mL^{-1}). Normal saline replaced BP-AgNPs in the control sample, and aspirin at 500 μg mL^{-1} concentration was utilized as the reference drug. After carefully inverting the tubes to mix the contents, all the tubes were submerged for 30 min in a water bath set at 56 °C. The reaction tubes were allowed to cool down after incubation and were later subjected to centrifugation at 2500 rpm for 10 minutes at room temperature. The absorbance of the supernatant was measured at 560 nm against normal saline blank.[25] To estimate the percentage inhibition from hemolysis, the following formula was employed.

© 2024 The Author(s). Published by the Royal Society of Chemistry

Open Access Article. Published on 01 jul 2024. Downloaded on 22.4.2026. 20.32.45.
This article is licensed under a Creative Commons Attribution-NonCommercial 3.0 Unported Licence.

$$\text{Percentage inhibition} = \left(\frac{\text{Absorbance of the control} - \text{Absorbance of the sample}}{\text{Absorbance of the control}}\right) \times 100$$

2.9.2.3 Hypotonicity-induced hemolysis. For this assay, 40% Human Red Blood Cells (HRBC) suspension was prepared in normal saline. 500 μL of various BP-AgNP concentrations (500–100 μg mL^{-1}) were mixed separately with 1000 μL of hypo-saline (0.36%). Lastly, 200 μL of a 40% HRBC solution was added to the reaction. Aspirin (500 μg mL^{-1}) was used as a standard drug after being dissolved in distilled water and for the control, hypo-saline was replaced with distilled water. All of the assay mixtures underwent a 30 minutes incubation period at 37 °C, after which a 10 minutes centrifugation at 2500 rpm was done. The supernatant's hemoglobin content was calculated at 540 nm spectrophotometrically against phosphate buffer blank.[26] In order to compute the hemolysis percentage, it was assumed that the amount of hemolysis that would occur in distilled water, being a hypotonic solution, would be 100% in the experimental setup.[27] The following equation was employed to calculate the percentage of hypotonicity-induced hemolysis inhibition.

$$\text{Percentage inhibition} = 100 - \left(\frac{\text{Absorbance of the sample}}{\text{Absorbance of the control}} \times 100\right)$$

2.10 Anti-glycation assay

2.10.1 BP-AgNPs incubation with *in vitro* glycation system. A BSA and fructose system was made for the anti-glycation assay, and the experiment was adopted from earlier research.[17] The experiment was conducted in capped autoclaved glass vials, and all the solutions were passed through a 0.22 micron syringe filter. Under a sterile environment, an aqueous solution of 30 mg mL^{-1} BSA was incubated with 1.5 M fructose (made in 0.1 M phosphate buffer pH 7.4) at room temperature. After that, BP-AgNPs (500–100 μg mL^{-1} concentrations prepared with 0.1 M phosphate buffer pH 7.4) was added and lastly, bacterial contamination was prevented by the addition of 0.5 mM sodium azide. The reaction volume was adjusted to 2 mL with the help of a buffer in the reaction vials, which were then incubated in a dark environment away from light at 37 °C for 7 days. The control was made with the same concentrations of reagents except AgNPs that were replaced by the buffer.

2.10.2 Determination of AGEs inhibition by fluorescence. After the incubation period, the fluorescence levels of glycated protein were assessed using a Thermo Scientific Varioskan LUX Microplate Reader. The specific excitation wavelength of 370 nm with emission measured at 440 nm was set to capture the fluorescence signals.[28] The following equation was applied to figure out the extent to which AGEs were formed in the presence of BP-AgNPs.

$$\%\text{AGEs formation} = \left(\frac{\text{Fluorescence intensity of the test sample}}{\text{Fluorescence intensity of the control}}\right) \times 100$$

2.11 Statistical analysis

The experimental results were conducted in triplicates ($n = 3$) and expressed as mean ± standard Error. The Plackett–Burman experimental design (PBD) was developed using Minitab 21 software; however, SPSS version 26 and One-Way ANOVA test was employed for statistical analysis. Following this, Tukey's post hoc was applied in experiments where equal variance was assumed and Games Howell for unequal variance. At p-values ≤ 0.01, the data was considered statistically significant.

3 Results and discussion

3.1 Phytochemical screening

The preliminary phytochemical study of the extract confirmed the presence of flavonoids, phenols, tannins, proteins and amino acids through the formation of color complexes in the reaction tubes, while the development of a stable foam after shaking the extract tube verified the presence of saponins. Moreover, a moderate amount of reducing sugar was also detected as the copper ions of Benedict's solution were reduced by the sugars to shift the color from blue to orange (ESI file†). The observed results for all the tests are illustrated in Table 3. The presence of flavonoids, tannins, phenols, saponins along with alkaloids in the banana peel extract was also evidenced by a study that reported AgNPs synthesis from *Musa balbisiana* species.[12]

3.2 Optimization through Plackett Burman design – design of experiments (PBD-DOE)

The DOE model with random combinations of factors were followed to carry out the reactions. The formation of silver nanoparticles was evidenced by color change and an absorption peak within the 400–475 nm region.[29] The λ_{max} of these reactions was identified to be at 427 nm; thus, the OD of all 39 trials was noted at this specific wavelength for PBD statistical analysis. The PBD outcomes presented in Table 4 revealed a wide range of diversity in AgNPs synthesis across these trials, spanning an absorbance range of 0.049–2.373. This is due to the combination of different variables that have their individual and combined effect on the synthesis of AgNPs. Each combination set resulted in differences in the nucleation and growth processes of the nanoparticles, ultimately resulting in

Table 3 Phytochemical analysis of banana peel extract

Phytochemicals test	Observation	Result
Quinones	No red color	−
Protein and amino acid	Yellow color	+
Flavonoids	Orange color	+
Reducing sugar	Orange color	+
Alkaloid	No blue color	−
Phlobatannins	No red precipitates	−
Tannins and phenols	Blue green, black color	+
Saponins	Stable foam	+
Tannins	Green precipitates	+
Phytosterol	No pink ring or red color	−

Open Access Article. Published on 01 jul 2024. Downloaded on 22.4.2026. 20.32.45.
This article is licensed under a Creative Commons Attribution-NonCommercial 3.0 Unported Licence.

Table 4 Response for the Plackett Burman design

Run order	Incubation time (hours)	Incubation temperature (°C)	$AgNO_3$ concentration (mM)	Plant extract : $AgNO_3$	OD_{427}
1	0.5	25	1	10	0.226
2	2	25	1	1	0.694
3	0.5	25	1	1	0.742
4	0.5	25	1	10	0.209
5	2	25	1	1	0.719
6	2	25	5	10	1.783
9	2	25	5	1	0.763
13	2	25	5	1	0.528
14	0.5	25	1	1	0.745
17	0.5	25	5	10	1.258
22	0.5	25	5	10	1.25
27	0.5	25	1	10	0.209
28	0.5	25	1	1	0.728
31	0.5	25	5	10	1.176
33	2	25	5	1	0.746
34	2	25	1	1	0.777
38	2	25	5	10	1.851
39	2	25	5	10	1.823
7	1.25	37.5	3	5.5	0.488
8	1.25	37.5	3	5.5	0.375
11	1.25	37.5	3	5.5	0.349
10	0.5	50	5	1	0.948
12	2	50	1	10	0.049
15	0.5	50	1	1	0.889
16	2	50	1	10	0.049
18	0.5	50	5	1	0.939
19	2	50	1	10	0.051
20	2	50	1	10	0.051
21	2	50	5	1	0.05
23	0.5	50	5	10	2.373
24	0.5	50	5	10	2.364
25	0.5	50	1	1	0.092
26	2	50	1	10	0.05
29	0.5	50	1	1	0.886
30	0.5	50	5	1	0.958
32	2	50	5	1	0.051
35	2	50	5	1	0.055
36	0.5	50	5	10	2.067
37	2	50	1	10	0.05

differences in their size, shape, and dispersion, which are reflected in the OD measurements. Also, the observed variation highlights the importance of optimizing factors in order to enhance AgNPs production.

3.3 Plackett Burman design statistical analysis

Minitab 21.0 was used to analyze the PBD. For the purpose of identifying significant variables and determining how they would affect the biosynthesis of AgNPs, the model summary, analysis of variance, Pareto chart, residual plot, and main effect plots were studied. The following is the regression equation that was generated,

$OD_{427} = 0.741 - 0.293$ incubation time $- 0.00946$ incubation temperature + 0.1912 $AgNO_3$ concentration + 0.0344 plant extract : $AgNO_3 - 0.379$ Ct Pt.

This equation creates a numerical relationship that corresponds to the response, explaining that if the concentration of $AgNO_3$ and plant extract-to-$AgNO_3$ ratio are increased to one unit then the OD or the synthesis of AgNPs would also increase by 0.19 and 0.034-fold, while the incubation temperature and time have the opposite effect, reducing them to low levels would result in a high response. However, Table 5 reveals that only the $AgNO_3$ concentration and incubation time variables are statistically significant.

According to the model summary, the R^2 value is 50%, indicating a moderately fit model. However, R^2 is only one metric for assessing the fitness of model to the data and it is always reliable to explore the residual plots to ensure that the model adheres to its underlying assumptions.

Model summary:

S	*R*-sq.	*R*-sq. (adj.)	*R*-sq. (pred.)
0.510376	50.51%	43.01%	33.20%

© 2024 The Author(s). Published by the Royal Society of Chemistry

Open Access Article. Published on 01 jul 2024. Downloaded on 22.4.2026. 20.32.45.
This article is licensed under a Creative Commons Attribution-NonCommercial 3.0 Unported Licence.

Table 5 Analysis of variance

Source	Degree of freedom (DF)	Adjusted sum of squares (Adj. SS)	Adjusted mean square (Adj. MS)	*F*-Value	*P*-Value
Model	5	8.7726	1.75452	6.74	0.000
Linear	4	8.3742	2.09355	8.04	0.000
Incubation time	1	1.7420	1.74196	6.69	0.014
Incubation temperature	1	0.5029	0.50292	1.93	0.174
$AgNO_3$ concentration	1	5.2647	5.26473	20.21	0.000
Plant extract : $AgNO_3$	1	0.8646	0.86459	3.32	0.078

It is evident from the residual plots in Fig. 1 that the data (response OD) are normally distributed because they closely align with the dotted line in the normal probability plot. The lack of a distinct bar that is far from the others in the histogram suggests that the data does not contain outliers. The residual *versus* fits plot shows that the residuals are randomly distributed with constant variance as the points are scattered on both sides of zero without any noticeable patterns. Similarly, the residual *versus* order plot indicates that the residuals are independent as they do not show any patterns or trends over time. Ideally, the residuals on the plot should demonstrate a random distribution along the center line.

By examining the normal probability plot of the effects, it is possible to determine the magnitude, direction, and significance of the effects (Fig. 2A). The half normal probability plot is another tool utilized to identify and select the most significant parameters. In both the plots, the variables that are lying closely to the straight line passing through zero are deemed non-significant, whereas the variables that are located farther away from the straight line are considered significant.[30] It shows that silver nitrate concentration and time are significant and have a greater impact on AgNPs concentration (Fig. 2B).

Pareto chart analysis was done to assess the significant variables involved in the AgNPs synthesis. A bar that crosses a designated cutoff line on the Pareto chart shows that the parameter is statistically significant. Pareto analysis (Fig. 3) demonstrated that the concentration of $AgNO_3$ is of greater significance for BP-AgNPs synthesis, followed by incubation time, whereas temperature and plant extract-to-$AgNO_3$ ratio were non-significant.

The main effects plot (Fig. 4) demonstrated the impact of different levels of factors involved in AgNPs synthesis on the OD regardless of their significance. 1 mM $AgNO_3$ concentration (level 1−) had almost no effect and 5 mM concentration (level 1+) had the greatest effect. Similarly, 0.5 hours incubation time had a higher effect than 2 hours incubation time. The values of significant factors with the highest mean response were chosen from the main effects plot. The final parameters chosen based on all the above-mentioned analysis are shown in Table 6.

Plackett Burman Design helped in identifying the significant factors and their individual effect on AgNPs synthesis. Previously, PBD has been utilized by several researchers to perform efficient green synthesis of AgNPs. In a study of lime peel extract (LPE)-AgNPs, the concentration of the precursor salt silver

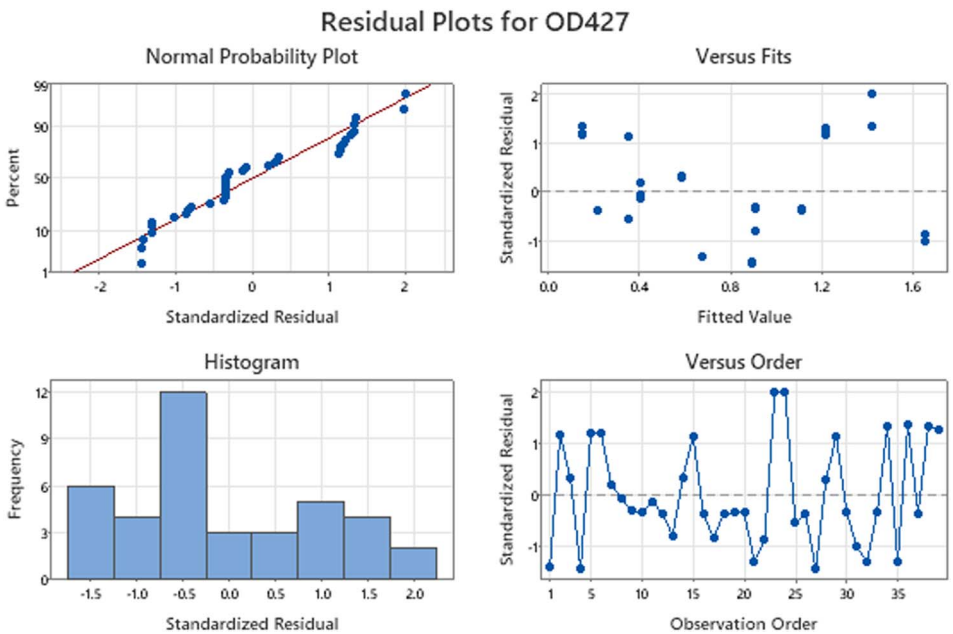

Fig. 1 Residual plots for OD_{427}. The plots demonstrates that the data provided for PDB analysis is normally distributed without outliers.

Open Access Article. Published on 01 jul 2024. Downloaded on 22.4.2026. 20.32.45.
This article is licensed under a Creative Commons Attribution-NonCommercial 3.0 Unported Licence.

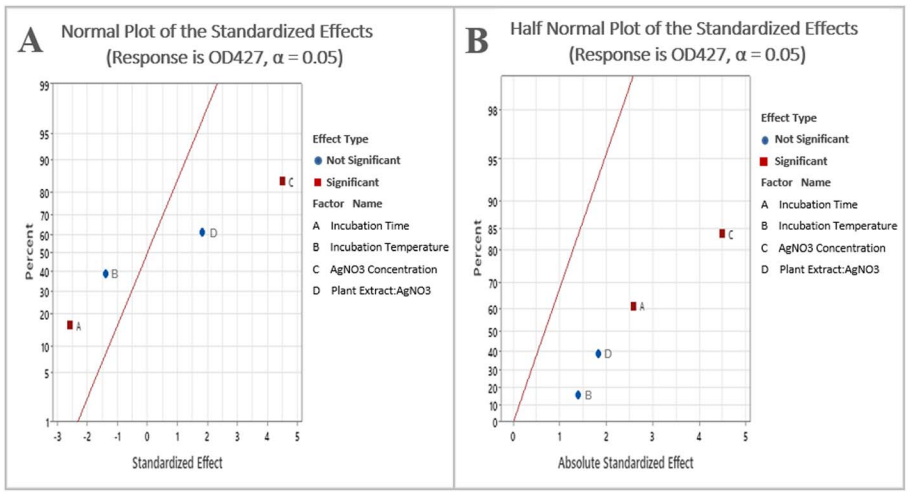

Fig. 2 (A) Normal plot of the standardized effects; (B) half normal plot of the standardized effects.

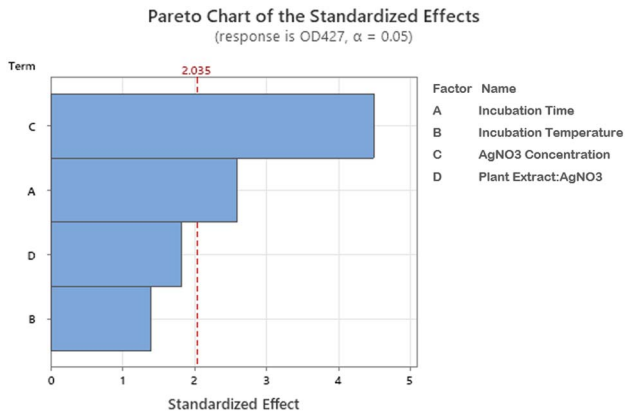

Fig. 3 Pareto chart of the standardized effects. The length of the factor bars shows their level of influence in BP-AgNP formation.

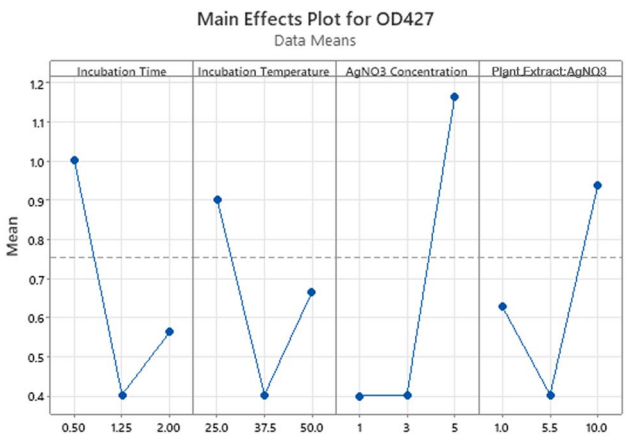

Fig. 4 Main effect plot for response at 427 nm shows the effects of all parameters regardless of the significance.

nitrate was observed to be the most significant factor, which is similar to the present study.[13] With that, Laime and colleagues reported pH and $AgNO_3$ concentration to be significant in their PBD-generated model for the synthesis of AgNPs through *Mutisia acuminatta* leaves.[8]

Table 6 Final parameters selected for the synthesis of BP-AgNPs

Parameters	Selected values
$AgNO_3$ concentration	5 mM
Incubation temperature	25 °C
Incubation time	0.5 hours
Plant extract : $AgNO_3$	1 : 10

3.4 Biosynthesis of AgNPs

After an incubation period of 30 min, the reaction mixture color changed from light yellow to dark brown, providing confirmation of the formation of BP-AgNPs, as seen in Fig. 5. The same trend was observed in Govindappa *et al.*'s investigation, who synthesized AgNPs using 5 mM $AgNO_3$ and *C. tomentosum* extract at room temperature (26 ± 2 °C). After a similar incubation period of 30 min, the λ_{max} appeared at 428 nm.[31]

The color shift observed upon the formation of BP-AgNPs resulted from the reduction of silver metal ions (Ag^+) into silver nanoparticles (Ag^0) through the involvement of active functional groups present in the banana peel extract (BPE). A hypothesis proposed that the polyphenols present in the plant-based extracts release reactive hydrogen through which polyphenols change to their keto-forms, thereby reducing Ag^+ to Ag^0.[3]

3.5 Characterization of banana peels-mediated AgNPs

3.5.1 Spectral analysis. The color shift after incubation is attributable to the excitation of surface plasmon resonance (SPR). The UV-Vis spectrum of the synthesized BP-AgNPs was studied in the wavelength range from 300 nm to 800 nm, as illustrated in Fig. 6. The BP-AgNPs demonstrated a peak in the 400–500 nm range with the λ_{max} at 427 nm. Numerous studies have reported the SPR maxima of AgNPs at 427 nm.[7,32]

© 2024 The Author(s). Published by the Royal Society of Chemistry

Open Access Article. Published on 01 jul 2024. Downloaded on 22.4.2026. 20.32.45.
This article is licensed under a Creative Commons Attribution-NonCommercial 3.0 Unported Licence.

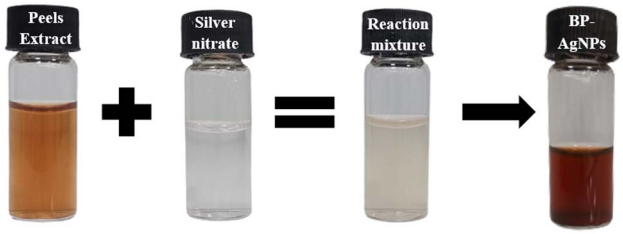

Fig. 5 Pictorial representation of BP-AgNPs synthesis. Extract combined with silver nitrate in a 1 : 10 ratio shows a pale color, which turned dark brown after incubation.

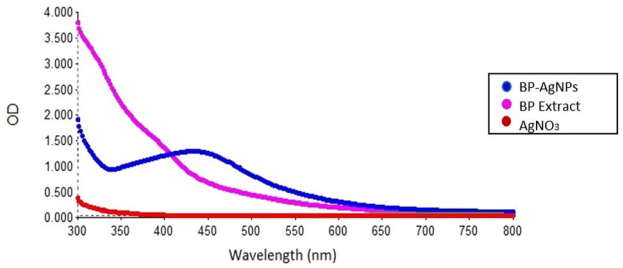

Fig. 6 UV-Vis spectrum of BP-AgNPs. The red line marks $AgNO_3$ absorption in the 300–800 nm range, pink represents the banana peel extract and blue BP-AgNPs.

3.5.2 SEM-EDX analysis of BP-AgNPs. Scanning electron microscopy (SEM) was employed to observe the morphology of the AgNPs. BP-AgNPs were clearly visible *via* SEM, proving their existence and poly-disperse nature. The size of the nanoparticles was observed in the range from 45 to 65 nm and they were primarily spherical (Fig. 7A). It is also visible that some nanoparticles were clumped together; this agglomeration was caused by a weak force of attraction between the nanoparticles, so they stick together while drying. The agglomeration of nanoparticles is commonly reported in the literature; lime peel-assisted AgNPs were also analyzed to be in the similar size range with slight agglomeration.[13]

Energy dispersive X-ray (EDX) analysis facilitated the determination of elemental composition and concentration, offering insights into the presence and abundance of specific elements involved in nanoparticles formation. Here, a sharp peak of Ag at 3 keV validates the existence of BP-AgNPs as metallic silver nanomaterials typically display this characteristic 3 keV peak in the optical absorption due to their surface plasmon resonance.[33] Silver by mass was found to be 86% and the rest 14% was oxygen, which might be present due to functional groups containing oxygen or surface oxidation (Fig. 7B). The elemental analysis through EDX conducted on nanoparticles derived from *Annona muricata* extract revealed 80% silver composition, which is similar to our study's findings.[7]

3.5.3 FTIR analysis for functional groups. Fourier transform infrared (FT-IR) spectroscopy analysis identified vibrational bonds near 1550 cm^{-1}, 1400 cm^{-1}, 1000 cm^{-1}, 800 cm^{-1} in both banana peels extract and BP-AgNPs spectra (Fig. 8). This gives important insights into the functional groups present on NPs surface and their contribution to nanoparticles formation. The broad peaks at 3330 cm^{-1} in plant extract was identified as the hydroxyl group, which refers to the phenolic groups, but it was not seen in the BP-AgNPs spectra.[29]

The peaks that occurred near 1550 cm^{-1} in both plant extract and BP-AgNPs were assumed to be caused by vibratory stretching within the N–C=O amide I bonds of proteins; the bands at 1400 cm^{-1} correspond to the C–H bending vibrations in the aromatic ring structures of tannins, bands at about 1000 cm^{-1} primarily arise from C–O stretching vibrations in aliphatic phenols and the minor peaks near 800 cm^{-1} might be due to the presence of gallotanins.[33,34] However, the area at 800 cm^{-1} or below is defined as the "skeletal region" because bands in this area are typically associated with the C–H bending or skeletal vibrations of carbohydrates, as their name implies.[35] In a study by Salve *et al.*, prominent peaks were observed at 1112 cm^{-1} and 1000 cm^{-1} due to the C=O stretching and bending of the C=C bond in AgNPs synthesized by *Madhuca longifolia* leaf extract, respectively. These spectral signatures are similar to that of BP-AgNPs and are indicative of the involvement of compounds such as flavonoids, carbohydrates and tannins.[4]

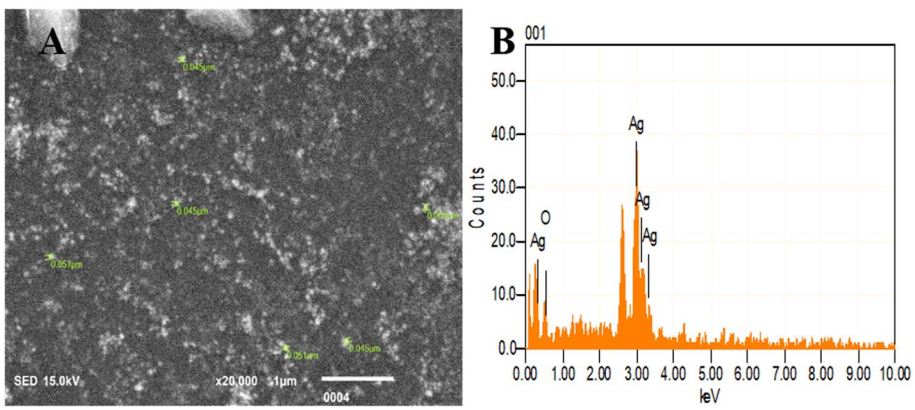

Fig. 7 SEM and EDX analysis of BP-AgNPs. (A) SEM image displaying the size of nanoparticles. (B) EDX indicating the elemental composition of the BP-AgNPs.

Open Access Article. Published on 01 jul 2024. Downloaded on 22.4.2026. 20.32.45.
This article is licensed under a Creative Commons Attribution-NonCommercial 3.0 Unported Licence.

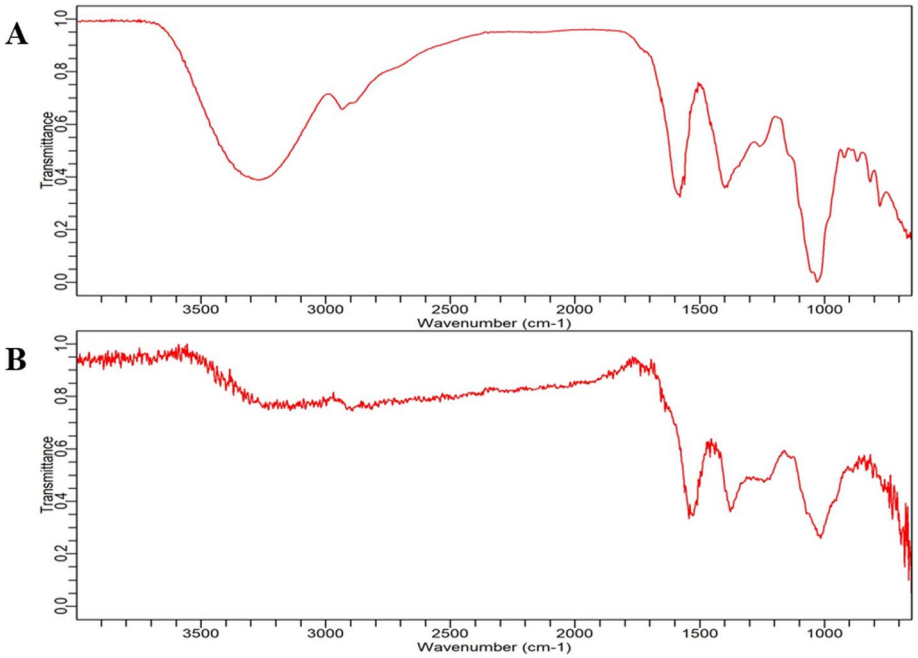

Fig. 8 FT-IR spectrum analysis. (A) Banana peel extract and (B) BP-AgNP spectrum in the range of 3500 cm^{-1} to 600 cm^{-1}.

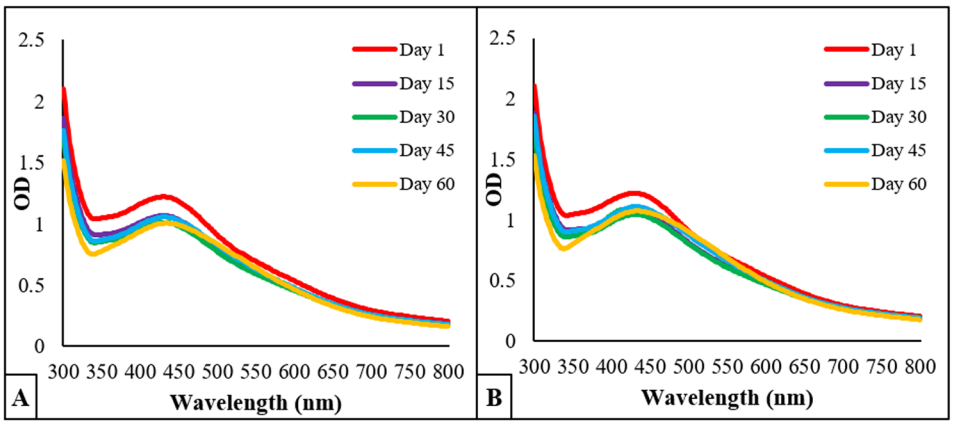

Fig. 9 Stability analysis of BP-AgNPs over the course of 60 days. (A) OD of BP-AgNPs at 4 °C and (B) OD of BP-AgNPs at room temperature.

3.6 Stability analysis

The stability studies of BP-AgNPs at 4 °C in refrigerator and room temperature revealed that the synthesized nanoparticles are fairly stable at both the conditions. Fig. 9A depicts the 4 °C stability graph in which the optical density of λ_{max} (427 nm) was 1.22 on day 1 and changed to 1.002 on day 60. However, at room temperature, the OD shifted from 1.22 to 1.07 after 60 days, as given in Fig. 9B. Following that, the λ_{max} gradually shifted to 432 nm; these minor differences in the absorption after 2 months showcased the stable nature of BP-AgNPs at both the conditions. In an earlier study, the stability of AgNPs obtained by the fruit extract of *Annona muricata* was also studied, reflecting their stable nature for 3 months at room temperature and 4 °C.[7]

3.7 Anti-oxidant activity through DPPH

The stable free radical 2,2-diphenyl-1-picrylhydrazyl (DPPH) is frequently employed to evaluate the antioxidant properties of different compounds, such as silver nanoparticles. This radical accepts an electron or hydrogen radical from the test antioxidant and consequently, it reduces to a distinctive yellow-colored compound known as diphenyl-picryl hydrazine, which can be measured by taking the absorbance at 517 nm.[16] Thus, through repeated experimentation, it was found that BP-AgNPs possess remarkable antioxidant activity. Ascorbic acid, which was used as the standard antioxidant agent, showed potent activity of 85% at 500 μg mL^{-1}, whereas BP-AgNPs showed 79% antioxidant activity at 500 μg mL^{-1}, which is close to that of ascorbic acid. The antioxidant activity gradually decreased in a dose-

© 2024 The Author(s). Published by the Royal Society of Chemistry

Open Access Article. Published on 01 jul 2024. Downloaded on 22.4.2026. 20.32.45.
This article is licensed under a Creative Commons Attribution-NonCommercial 3.0 Unported Licence.

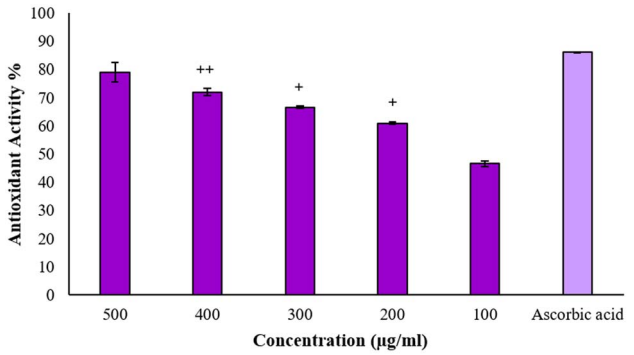

Fig. 10 Antioxidant activity of BP-AgNPs and ascorbic acid. The + symbol denotes significance in comparison with the 100 µg mL^{-1} concentration.

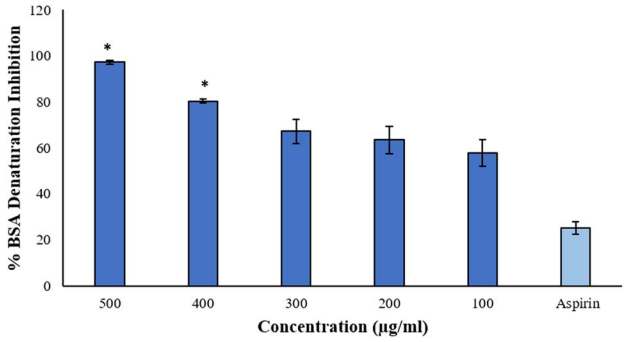

Fig. 11 Percentage of BSA denaturation inhibition. *x*-axis indicates the different concentrations of BP-AgNPs and aspirin (500 µg mL^{-1}). The symbol * represents statistical significance with respect to the standard.

dependent manner, reaching 46% at 100 µg mL^{-1}, as shown in Fig. 10. When different concentrations of the BP-AgNPs were compared for a significant difference in activity, it was found that in comparison to 100 µg mL^{-1}, all other concentrations from 200–400 µg mL^{-1} showed significantly high antioxidant activity (p value $\leq$ 0.01 for 200 and 300 µg mL^{-1} and p value $\leq$ 0.001 for 400 µg mL^{-1}, respectively).

The results obtained are better than the previous findings of plants extracts-aided AgNPs as the AgNPs from *Alternanthera sessilis* showed a dose-dependent increase in the antioxidant activity with the maximum of 62% at 500 µg mL^{-1}.[36] The stem and leaves extract of *Clinacanthus nutans* were used to form silver nanoparticles that displayed 49.94% and 51.39% antioxidant activity at 500 µg mL^{-1}, respectively.[37] In another study, the reducing agent utilized was *Melia azedarach* extract for stable AgNPs formation at room temperature, where the antioxidant activity at 500 µg mL^{-1} was found to be 63.83%.[38]

3.8 Anti-inflammatory assays

3.8.1 Protein denaturation inhibition. Protein denaturation occurs when the secondary and tertiary structures of proteins get disturbed due to external stress like concentrated salts, acids/bases or heat. This also interferes with the proteins' quaternary structure, causing aggregation that triggers injurious inflammatory signals.[39] Albumin is a common protein found nearly in all the animals; thus, Bovine Serum Albumin (BSA) was the assay's reagent. Heat denatures BSA and triggers the expression of antigens that are involved in inflammatory responses.[16] Thus, the anti-inflammatory response capability of BP-AgNPs was evaluated through BSA, and some noteworthy results were obtained. It was found that the nanoparticles at the highest concentration of 500 µg mL^{-1} protect 97% of the BSA against denaturation by heat. The percentage inhibition gradually decreased to 57% at 100 µg mL^{-1}, which was again better inhibition than the standard drug (aspirin), which was found to be 25% at 500 µg mL^{-1}, as depicted in Fig. 11. In comparison to aspirin, 500 µg mL^{-1} and 400 µg mL^{-1} concentration of BP-AgNPs demonstrated significantly high inhibition activity (p value $\leq$ 0.01).

The data is in good agreement with the earlier findings that involved a medicinal plant *Cissus quadrangularis*-derived AgNPs, in which the percentage inhibition of BSA denaturation was recorded to be 85% at 500 µg mL^{-1},[9] while *Brachychiton populneus*-assisted silver nanoparticles inhibited 81.13% of albumin denaturation at the maximum concentration of 500 µg mL^{-1}.[40] However, AgNPs at 600 µg mL^{-1} synthesized from tamarix aqueous extract expressed 73.19% of inhibition.[27]

3.8.2 Heat-induced hemolysis inhibition. The stabilization of lysosomal membranes when stressed could prevent enzyme release and subsequent inflammation. This serves as a model to use erythrocyte membranes to assess the anti-inflammatory activity as they mimic the lysosomal membrane.[41] AgNPs synthesized using plant sources can aid by maintaining the fluidity and ion balance, enhancing the biomembrane stability or neutralizing the lysosomal enzyme activity.[42] Therefore, BP-AgNPs were tested against heat as one of the stress conditions. The hemolysis protection by heat was 90% at 500 µg mL^{-1} BP-AgNPs that eventually decreased to 39% at 100 µg mL; these results were significantly higher than the standard that showed 66% protection at 500 µg mL^{-1} concentration (Fig. 12A and B). The BP-AgNPs at 500 µg mL^{-1} and 400 µg mL^{-1} concentration demonstrated significant difference in the hemolysis inhibition compared to the standard (p value $\leq$ 0.001 at 500 µg mL^{-1} and p value $\leq$ 0.01 at 400 µg mL^{-1} respectively). In comparison to 100 µg mL^{-1} concentration of BP-AgNPs, a significantly high activity (p value $\leq$ 0.000) was observed in all the other concentrations of BP-AgNPs. The study reported by Anwar *et al.* demonstrated 74.16% of heat-hemolysis inhibition at 600 µg mL^{-1} concentration of tamarix-mediated AgNPs, which was similar to that of aspirin (75% at 200 µg mL^{-1}).[27] The silver nanoparticles derived from *Calophyllum tomentosum* showed 84% of hemolysis protection at 100 µg mL^{-1}.[31] It is possible that the AgNPs stabilized the membranes of red blood cells by blocking the release of active inflammation mediators and lytic enzymes.

3.8.3 Hyposalinity-induced hemolysis inhibition. In hyposalinity-hemolysis inhibition assay, the hypotonic solution causes the RBCs to absorb the excess fluid, which swells up the cell membrane, leading to their rupture. By stabilizing the membrane, BP-AgNPs may restrict fluid and serum protein

Open Access Article. Published on 01 jul 2024. Downloaded on 22.4.2026. 20.32.45.
This article is licensed under a Creative Commons Attribution-NonCommercial 3.0 Unported Licence.

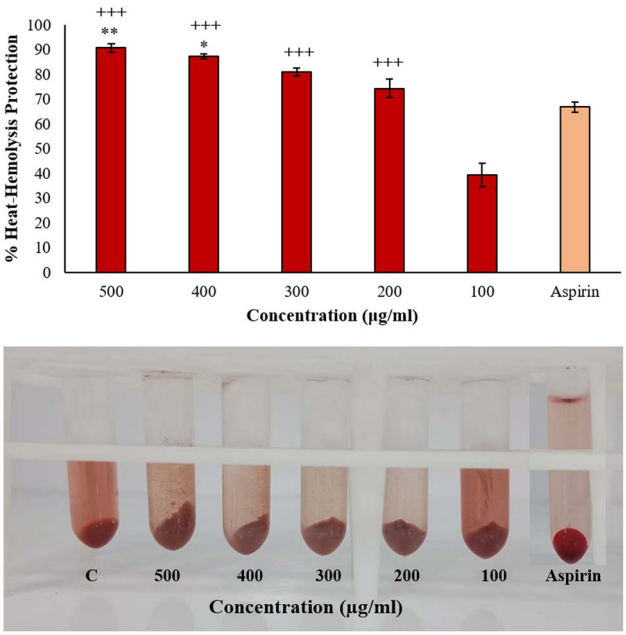

Fig. 12 Heat induced hemolysis protection. The *x*-axis of the bar graph shows the concentrations of BP-AgNPs and aspirin (500 µg mL^{-1}). The symbol * represents the statistically significant difference compared to standard whereas + sign represents significance in comparison to 100 µg mL^{-1}. The pictorial representation demonstrates the heat induced hemolysis inhibition of aspirin (500 µg mL^{-1}) and different concentrations of BP-AgNPs. The symbol C represents the control.

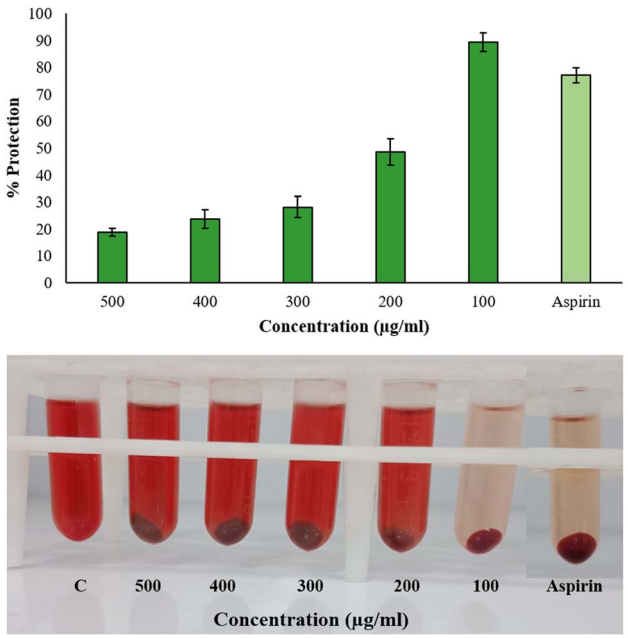

Fig. 13 Hyposalinity induced hemolysis percentage inhibition. The *x*-axis of the bar graph shows the concentrations of BP-AgNPs and the lighter colored bar represents 500 µg mL^{-1} of aspirin. In pictorial illustration of hyposalinity induced hemolysis inhibition, the symbol C represents the control with no inhibitor and aspirin was tested at a concentration of 500 µg mL^{-1}.

leaks into the tissues that are brought on by hyposalinity. Hence, the hemolysis inhibition activity of BP-AgNPs was tested and a higher level of protection was seen with BP-AgNPs than aspirin. At 500 µg mL^{-1} concentration of BP-AgNPs, 18% of hemolysis protection was observed, which increased at lower concentrations; thereby, at 100 µg mL^{-1} concentration, 89% of hemolysis protection was observed. However, the standard drug aspirin protected 77% of erythrocytes against hyposalinity stress, as depicted in Fig. 13A and B.

The results did not follow a dose-dependent pattern, and a green synthesis study of copper nanoparticles showed similar behavior, wherein the hemolysis inhibition under hypotonic treatment was high at 50 µg mL^{-1} than 200 µg mL^{-1}.[43] This suggests that there are other factors that have pivotal roles in nanoparticles interaction with the environment to influence hemolysis than merely the concentration. Nanoparticles might saturate the available interaction sites or agglomerate at high concentration while at lower concentrations, more surface-to-volume ratio is available for interaction in a hypotonic environment. AgNPs might as well compete for binding sites, hindering the individual effectiveness in stabilizing the membranes. Additionally, reduced ionic strength in low-salinity conditions may lessen the electrostatic repulsion, which could lead to nanoparticle precipitation or aggregation. Some earlier reports showed that the percentage of membrane stabilization by *S. khasianum* methanolic extract-derived AgNPs at 200–1000 µg mL^{-1} concentration was 62.6% to 84%.[44] At 1 mg mL^{-1}, *Nothapodytes foetida*-aided silver nanoparticles had a maximal protection activity of 89% in hypo-saline medium.[45]

3.9 Anti-glycation assay

Advanced glycation end products or AGEs are produced when lipids, proteins and DNA non-enzymatically bind with sugar molecules. AGEs formation and accumulation inside the body is linked with the sugar concentration and its stay duration and numerous AGEs are associated with several clinical diseases.[17] Anti-glycation studies reveal that BP-AgNPs possess significant anti-glycation activity. The control without the inhibitor turned golden yellow after the incubation period, marking the formation of AGEs, thus producing maximum fluorescence intensity.

After a 7 days incubation period, only 4% AGEs were able to form due to the effectiveness of BP-AgNPs at 500 µg mL^{-1} concentration, which reflects the potent nature of BP-AgNPs in suppressing AGEs formation. As depicted in Fig. 14, the AGEs percentage increased as the BP-AgNPs concentration decreased but even at the lowest concentration of 100 µg mL^{-1}, the AGEs percentage increased from 4% to 13%, only reflecting the extraordinary AGEs inhibition property of BP-AgNPs. At all the tested concentrations, AgNPs demonstrated a substantial decrease in the generation of AGEs when compared to the control (p value $\leq$ 0.000 for 500 µg mL^{-1} to 200 µg mL^{-1} and p value $\leq$ 0.001 for 100 µg mL^{-1}). In a study, green-synthesized AgNPs from *Moringa oleifera* displayed 84% AGEs inhibition, which is equal to 16% of AGEs formation at 500 µg mL^{-1}.[28] *Eysenhardtia polystachya*-fabricated AgNPs demonstrated 38% to 52% AGEs

© 2024 The Author(s). Published by the Royal Society of Chemistry

Open Access Article. Published on 01 jul 2024. Downloaded on 22.4.2026. 20.32.45.
This article is licensed under a Creative Commons Attribution-NonCommercial 3.0 Unported Licence.

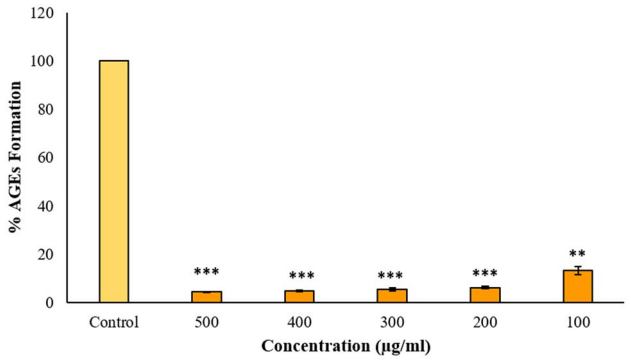

Fig. 14 Anti-glycation activity. The *x*-axis specifies the concentrations of BP-AgNPs (500–100 µg mL^{-1}), whereas the lighter color bar is the control containing BSA and glucose without any inhibitor. * indicates the statistical significance of BP-AgNPs in lowering the AGEs formation when compared to the control.

formation at 500–2000 µg mL^{-1} after 4 weeks of incubation.[46] These reports signify the enhanced anti-glycation efficacy of BP-AgNPs.

4 Conclusion

The investigation was conducted to record the therapeutic potential of the silver nanoparticles synthesized *via* a green approach employing banana peels extract. The optimization of the synthesis parameters by the innovative Plackett Burman Design of experiments revealed a significant enhancement in AgNPs production efficiency with minimal time and energy consumption. The synthesized BP-AgNPs were spherically shaped in SEM analysis and a fair share of 86% silver element was seen in the EDX analysis. The involvement of phenols, tannins and carbohydrates in the reduction and stabilization of nanoparticles was identified through FTIR and phytochemical screening. The radical scavenging ability against DPPH was found to be 79% at 500 µg mL^{-1} concentration of AgNPs. Different anti-inflammatory assays were conducted against erythrocytes and BSA, displaying significant results when compared to the standard drug aspirin. Lastly, the antiglycation activity was notably high as only 4% AGEs were formed at 500 µg mL^{-1} concentration. The study unveils the promising activity of banana peels-assisted silver nanoparticles in combating oxidative stress-related diseases, encompassing novel anti-inflammatory and anti-glycation activity. This suggests the potential use of BP-AgNPs as a therapeutic agent or drug conjugate for enhanced efficacy.

Data availability

The data supporting this article are included as part of ESI.†

Author contributions

Madiha M. Fazil: conceptualization, methodology, software, validation, formal analysis, investigation, data curation, writing – original draft, writing – review & editing, visualization, project administration. Anum Gul: conceptualization, methodology, software, validation, writing – review & editing, visualization, project administration, supervision, resources, funding acquisition. Huma Jawed: methodology, validation, writing – review & editing, visualization, project administration, supervision, resources, funding acquisition.

Conflicts of interest

The authors affirm that the work reported in this study was conducted without any known competing financial interests or personal relationships that could have influenced its outcomes.

References

1 X.-F. Zhang, *et al.*, Silver nanoparticles: synthesis, characterization, properties, applications, and therapeutic approaches, *Int. J. Mol. Sci.*, 2016, **17**(9), 1534.
2 M. Kushwah, *et al.*, Antibacterial and antioxidant activity of biosynthesized silver nanoparticles produced by Aegle marmelos fruit peel extract, *Anal. Chem. Lett.*, 2019, **9**(3), 329–344.
3 V. Makarov, *et al.*, "Green" nanotechnologies: synthesis of metal nanoparticles using plants, *Acta Naturae*, 2014, **6**(20), 35–44.
4 P. Salve, *et al.*, An evaluation of antimicrobial, anticancer, anti-inflammatory and antioxidant activities of silver nanoparticles synthesized from leaf extract of Madhuca longifolia utilizing quantitative and qualitative methods, *Molecules*, 2022, **27**(19), 6404.
5 R. E. Morsi, *et al.*, Multifunctional nanocomposites of chitosan, silver nanoparticles, copper nanoparticles and carbon nanotubes for water treatment: antimicrobial characteristics, *Int. J. Biol. Macromol.*, 2017, **97**, 264–269.
6 B. S. Sekhon, *Nanotechnology in Agri-Food Production: an Overview. Nanotechnology, Science and Applications*, 2014, pp. 31–53.
7 Y. Gavamukulya, *et al.*, Green synthesis and characterization of highly stable silver nanoparticles from ethanolic extracts of fruits of Annona muricata, *J. Inorg. Organomet. Polym. Mater.*, 2020, **30**(4), 1231–1242.
8 L. A. Laime-Oviedo, *et al.*, Plackett-Burman design in the biosynthesis of silver nanoparticles with Mutisia acuminatta (Chinchircoma) and preliminary evaluation of its antibacterial activity, *F1000Research*, 2023, **12**, 1462.
9 S. Kanimozhi, *et al.*, Biogenic synthesis of silver nanoparticle using Cissus quadrangularis extract and its invitro study, *J. King Saud Univ. Sci.*, 2022, **34**(4), 101930.
10 S. F. Sulaiman, *et al.*, Correlation between total phenolic and mineral contents with antioxidant activity of eight Malaysian bananas (Musa sp.), *J. Food Compos. Anal.*, 2011, **24**(1), 1–10.
11 R. Suhag, *et al.*, Fruit peel bioactives, valorisation into nanoparticles and potential applications: A review, *Crit. Rev. Food Sci. Nutr.*, 2022, 1–20.
12 S. S. Bag, A. Bora and A. K. Golder, Biomimetic synthesis of silver nanoparticles using bhimkol (Musa balbisiana) peel

Open Access Article. Published on 01 jul 2024. Downloaded on 22.4.2026. 20.32.45.
This article is licensed under a Creative Commons Attribution-NonCommercial 3.0 Unported Licence.

extract as biological waste: Its antibacterial activity and role of ripen stage of the peel, *Curr. Nanomater.*, 2020, **5**(1), 47–65.

13 A. Naysmith, N. S. Mian and S. Rana, Development of conductive textile fabric using Plackett–Burman optimized green synthesized silver nanoparticles and in situ polymerized polypyrrole, *Green Chem. Lett. Rev.*, 2023, **16**(1), 2158690.

14 J. Zhou, *et al.*, Optimization of phenol degradation by Candida tropicalis Z-04 using Plackett-Burman design and response surface methodology, *J. Environ. Sci.*, 2011, **23**(1), 22–30.

15 M. M. Yallapu, *et al.*, Implications of protein corona on physico-chemical and biological properties of magnetic nanoparticles, *Biomaterials*, 2015, **46**, 1–12.

16 S. Anwar, *et al.*, Protective effects of ginger extract against glycation and oxidative stress-induced health complications: An in vitro study, *Processes*, 2020, **8**(4), 468.

17 W. Wang, *et al.*, Phytochemicals from berries and grapes inhibited the formation of advanced glycation end-products by scavenging reactive carbonyls, *Food Res. Int.*, 2011, **44**(9), 2666–2673.

18 S. Bhatt and S. Dhyani, Preliminary phytochemical screening of Ailanthus excelsa Roxb, *Int. J. Curr. Pharm. Res.*, 2012, **4**(1), 87–89.

19 G. O. De Silva, A. T. Abeysundara and M. M. W. Aponso, Extraction methods, qualitative and quantitative techniques for screening of phytochemicals from plants, *Am. J. Essent. Oil. Nat. Prod.*, 2017, **5**(2), 29–32.

20 T. Tyagi, Phytochemical screening of active metabolites present in Eichhornia crassipes (Mart.) Solms and Pistia stratiotes (L.): Role in ethanomedicine, *Asian J. Pharm. Educ. Res.*, 2017, **6**(4), 40–56.

21 M. S. Auwal, *et al.*, Preliminary phytochemical and elemental analysis of aqueous and fractionated pod extracts of Acacia nilotica (Thorn mimosa), in *Veterinary research forum: an international quarterly journal*, Faculty of Veterinary Medicine, Urmia University, Urmia, Iran, 2014.

22 R. María, *et al.*, Preliminary phytochemical screening, total phenolic content and antibacterial activity of thirteen native species from Guayas province Ecuador, *J. King Saud Univ. Sci.*, 2018, **30**(4), 500–505.

23 M. A. Alsahli, *et al.*, 6-Gingerol, a major ingredient of ginger attenuates diethylnitrosamine-induced liver injury in rats through the modulation of oxidative stress and anti-inflammatory activity, *Mediators Inflammation*, 2021, **2021**, 1–17.

24 A. H. Rahmani, *et al.*, Therapeutic Potential of Myrrh, a Natural Resin, in Health Management through Modulation of Oxidative Stress, Inflammation, and Advanced Glycation End Products Formation Using In Vitro and In Silico Analysis, *Appl. Sci.*, 2022, **12**(18), 9175.

25 S. Sakat, A. R. Juvekar and M. N. Gambhire, In vitro antioxidant and anti-inflammatory activity of methanol extract of Oxalis corniculata Linn, *Int. J. Pharmacol. Pharm. Sci.*, 2010, **2**(1), 146–155.

26 M. S. Parvin, *et al.*, Evaluation of in vitro anti-inflammatory and antibacterial potential of Crescentia cujete leaves and stem bark, *BMC Res. Notes*, 2015, **8**, 1–7.

27 S. Anwar, *et al.*, Biosynthesis of silver nanoparticles using Tamarix articulata leaf extract: An effective approach for attenuation of oxidative stress mediated diseases, *Int. J. Food Prop.*, 2021, **24**(1), 677–701.

28 D. Verma, *et al.*, In vitro anti-arthritic and antiglycation potential of a combination of silver nanoparticles and Moringa oleifera leaves extract, *Nanomed. J.*, 2022, **9**(4), 334–344.

29 R. Gul, *et al.*, Eco-friendly synthesis of silver nanoparticles and its biological evaluation using Tamarix aphylla leaves extract, *Mater. Technol.*, 2022, **37**(9), 962–969.

30 E. Aghaie, *et al.*, Response surface methodology (RSM) analysis of organic acid production for Kaolin beneficiation by Aspergillus niger, *Chem. Eng. J.*, 2009, **147**(2–3), 245–251.

31 M. Govindappa, *et al.*, Characterization, antibacterial, antioxidant, antidiabetic, anti-inflammatory and antityrosinase activity of green synthesized silver nanoparticles using Calophyllum tomentosum leaves extract, *Results Phys.*, 2018, **9**, 400–408.

32 T. T. Trung, *et al.*, Study on synthesizing silver nanoparticles by using Muntingia calabura leaf extract: Insights from experimental and theoretical studies, *Vietnam J. Chem.*, 2021, **59**(5), 606–611.

33 H. M. Ibrahim, Green synthesis and characterization of silver nanoparticles using banana peel extract and their antimicrobial activity against representative microorganisms, *J. Radiat. Res. Appl. Sci.*, 2015, **8**(3), 265–275.

34 A. Koochakzaei and M. Sabaghian, Tannin characterization and sourcing in historical leathers through FTIR spectroscopy and PCA analysis, *Collagen Leather*, 2023, **5**(1), 21.

35 E. Wiercigroch, *et al.*, Raman and infrared spectroscopy of carbohydrates: A review, *Spectrochim. Acta, Part A*, 2017, **185**, 317–335.

36 K. Niraimathi, *et al.*, Biosynthesis of silver nanoparticles using Alternanthera sessilis (Linn.) extract and their antimicrobial, antioxidant activities, *Colloids Surf., B*, 2013, **102**, 288–291.

37 H. I. Chiu, *et al.*, Biogenic silver nanoparticles of Clinacanthus nutans as antioxidant with antimicrobial and cytotoxic effects, *Bioinorg. Chem. Appl.*, 2021, **2021**, 1–11.

38 G. Chinnasamy, S. Chandrasekharan and S. Bhatnagar, Biosynthesis of silver nanoparticles from Melia azedarach: Enhancement of antibacterial, wound healing, antidiabetic and antioxidant activities, *Int. J. Nanomed.*, 2019, 9823–9836.

39 S. Prabhu and E. K. Poulose, Silver nanoparticles: mechanism of antimicrobial action, synthesis, medical applications, and toxicity effects, *Int. Nano Lett.*, 2012, **2**, 1–10.

40 M. Naveed, *et al.*, Characterization and evaluation of the antioxidant, antidiabetic, anti-inflammatory, and cytotoxic activities of silver nanoparticles synthesized using

© 2024 The Author(s). Published by the Royal Society of Chemistry

Open Access Article. Published on 01 jul 2024. Downloaded on 22.4.2026. 20.32.45.
This article is licensed under a Creative Commons Attribution-NonCommercial 3.0 Unported Licence.

Brachychiton populneus leaf extract, *Processes*, 2022, **10**(8), 1521.

41 S. Vijayakumar, *et al.*, Biological compound capping of silver nanoparticle with the seed extracts of blackcumin (Nigella sativa): a potential antibacterial, antidiabetic, anti-inflammatory, and antioxidant, *J. Inorg. Organomet. Polym. Mater.*, 2021, **31**, 624–635.

42 O. Amujoyegbe, *et al.*, In vitro evaluation of membrane stabilizing activities of leaf and root extracts of Calliandra portoricensis (JACQ) benth on sickle and normal human erythrocytes, *Int. J. Pharmacol. Pharm. Res.*, 2012, **2**(8), 198–203.

43 S. Rajeshkumar, *et al.*, Anti-inflammatory and antimicrobial potential of Cissus quadrangularis-assisted copper oxide nanoparticles, *J. Nanomater.*, 2021, **2021**, 1–11.

44 P. Chirumamilla, *et al.*, In vitro anti-inflammatory activity of green synthesized silver nanoparticles and leaf methanolic extract of Solanum khasianum Clarke, *Proc. Natl. Acad. Sci., India, Sect. B*, 2022, **92**(2), 301–307.

45 S. B. Dharavath, P. Chirumamilla and S. Taduri, Evaluation of antioxidant, anti-inflammatory and antidiabetic activities of green synthesized silver nanoparticles and in vivo plant extracts of Nothapodytes foetida, *Vegetos*, 2023, **36**(3), 920–928.

46 R. M. P. Gutierrez, *et al.*, Silver nanoparticles synthesized using Eysenhardtia polystachya and assessment of the inhibition of glycation in multiple stages in vitro and in the Zebrafish Model, *J. Cluster Sci.*, 2018, **29**, 1291–1303.